Modelling semi-rigid composite joints with precast hollowcore slabs in hogging moment region

Feng Fu*, Dennis. Lam[1] and Jianqiao Ye[1]

Abstract

In this paper, using the general purpose software ABAQUS, a three dimensional (3-D) finite element model was built to simulate semi-rigid composite connection with precast hollowcore slabs. 3D continuums elements are used for all parts of the composite connections and the contact conditions between all the components are explicitly modelled. The model also incorporates nonlinear material characteristics and non-linear geometric behaviour. A simplified method to simulate the bolted end plate connection is introduced and validated. The proposed simulation method of the longitudinal shear transmission can accurately simulate the plastic state of the longitudinal rebars after cracking. Different materials are chosen by the authors to simulate the concrete slab and the elastic-plastic material property is adopted which can accurately simulate the moment-rotation response of the connections. Numerical results are presented and compared with the experimental data and good agreement is obtained.

Keywords*: connection, semi-rigid, pretension,* finite element; connections; modelling; bolts;

* Corresponding author
E-mail address: cenffu@yahoo.co.uk
WSP Group Ltd. Buchanan House,24-30 Holborn,EC1N 2HS,London,United Kingdom
[1]School of Civil Engineering, University of Leeds, Leeds, LS2 9JT, U.K.

1. Introduction

In the design of multi-storey buildings, it is more realistic to consider the composite connection behaves semi-rigid. The advantages of design semi-rigid connections have been well recognized by the designers for a long time. It will reduce beam weight, which in turn will reduce the beam depth, the overall building height and cladding cost, etc. Compare to the pin support, it can also improve serviceability performance due to the increased stiffness; provide greater robustness as a result of improved continuity between frame members and better crack control in the floor slabs. Although the effect of semi-rigid composite connections on the structural behaviour and their potential economical benefits is well recognized, all the slabs currently used are either solid slab or metal decking. Little research has been done toward the semi-rigid composite connections with precast hollowcore slabs.

To investigate the structural behaviour of the semi-rigid connection, the most important issue is the moment-rotation response of the connection. One of the effective research methods is through full scale testing. Eight full scale tests have been conducted by Fu and Lam [1] to investigate the moment-rotation response of semi-rigid composite connection with precast hollowcore slabs. However, due to the cost limitation of tests, only a small number of parameters can be taken into account. Non-linear finite element modelling is an attractive tool for modelling connections. Use of finite element modelling could explore large number of variables and potential failure modes, which could complement the experimental studies. Therefore, the

combined experimental / numerical approach is an extremely powerful way to develop a full understanding of complex structural behaviour.

In the history of the Finite element modelling studies of steel beam to column connections, Krishnamurthy[2][3]was the pioneer in the field of 3-D modelling of connections, by adopting eight-node sub-parametric bricks in order to reproduce the behaviour of bolted end plate connections. The analysis carried out were linearly elastic but computational expensive because contact was embodied artificially by attaching and releasing nodes at each loading step on the basis of the stress distribution, bolt preloading phenomena were also simulated. Correlation between two-dimensional 2-D and 3-D finite element analysis was established and a parametric study was conducted with the 2-D models. A 3-D finite element model based on solid and contact elements of the ABAQUS [4] were proposed by Bursi et al. [5] to simulate the rotational behaviour of isolated bolted end plate connections and they discussed the basic issues such as constitutive relationships, step size, number of integration points, kinematic descriptions, element types and discretizations for the modelling of the endplate connection. Choi et al.[6] proposed a refined 3-D finite element model for endplate connections. Ayoub and Filippou [7] presented an inelastic beam element for the analysis of steel–concrete composite girders with partial composite action under monotonic and cyclic loads. This element was derived from a two-field mixed formulation. Fibre discretization of section and hysteric material models for the constituent materials are used to achieve the nonlinear response. Sebastian and McConnel [8] developed another beam element with layered

steel beams and layered concrete slabs for the analysis of steel–concrete composite girders. In their study, they also included modelling of the profiled steel sheeting. A specialized stub element with an empirical nonlinear shear force–slip relationship is used at the concrete slab–steel beam interface to permit the modelling of either full or partial shear connections. A specific kinematic model of the cross section is proposed by Fabbrocino et al. [9] for the analysis of continuous composite beams including partial interaction and bond. A simple 2-D model has been made for the analysis of composite connections and composite frames by Ahmed [10] using ABAQUS. In his model, he ignored the concrete slab under negative bending and analyzed the steel beam with multipoint constraint to behave like a composite girder. Baskar et al. [11] built up a 3-D finite element model using ABAQUS. The model has been used to analyze the steel-concrete composite plate girders under negative bending and shear loading. In order to overcome the convergence problem of the concrete material under the negative bending conditions, different element types and material properties were tried to simulate the concrete slab. Modelling of the headed studs in steel-precast composite beams using the finite element analysis software ABAQUS was carried out by El-Lobody and Lam [12] and good agreement was obtained in comparison to the test results. Ju et. al [13] used the three-dimensional (3D) elasto-plastic finite element method to study the structural behaviour of the butt-type steel bolted joint. The numerical results are compared with AISC specification data. The similarity was found to be satisfactory despite the complication of stress and strain fields during the loading stages. Vigh et. al [14] used the programme language MATLAB to create the

script-file that is directly readable by ANSYS. They built up the entire numerical model of the bolted joints. To simulate the bolted endplates connections, the endplate are connected by linear tension-only spring elements (element type LINK10 [4]) acting for the bolts. The rigid compression-only elements (LINK10) are used to represent the contact phenomenon between the two endplates. Additionally, further links (coupled nodes) are used to avoid the lateral slide of endplates on each other. The model provided satisfactory results. Kumar et. al [15] conducted finite element modelling of the beam-to-column connection with web opening using the finite element analysis software MSC/NASTRAN. The component plates of the beam, column, and the channel connectors were discretised using isoparametric four-node quadrilateral plate elements. Finer mesh was used in the connection region to get the magnitude of the stress concentration accurately. The beam web was not connected to the column. The effect of HSFG bolts was represented by the use of rigid elements connecting the corresponding nodes on the beam flange and the channel connector, so as to simulate no-slip condition and to transmit the beam flange force to the channel connector. Bolt slip has not been modelled. The bearing action of the RHS beam on the channel connectors during bending of the beam was simulated using spring elements of high compressive stiffness. The model is also accurate enough compared with the experiment tests.

In the past two decades, many theoretical research of the semi-rigid composite connection was done by researchers European Union. Anderson [16] conducted the research on composite steel-concrete joints in braced frames for buildings. Jaspart [17]

summarized the advances in the field of structural steel joints and their representation in the building frame analysis and design process. Based on these research findings, the mechanical model using the component method was proposed in EC3 [18] and EC4 [19]. This is a significant achievement in the study of the composite connections. The principle of this method is to divide the connection into a set of mechanically connected components, representing the behaviour of elemental parts. The behaviour of each element is then described by general constitutive relations, either in stress space or strain space. Finally, the general connection behaviour can be combined together from these separate element relationships by considering force equilibrium and deformation compatibility. Braconi et al [20] proposed a refined component model to predict the inelastic monotonic response of exterior and interior beam-to-column joints for partial-strength composite steel–concrete moment-resisting frames. The joint typology is designed to exhibit ductile seismic response through plastic deformation developing simultaneously in the column web panel in shear, the bolted end-plate connection, the column flanges in bending and the steel reinforcing bars in tension. The model can handle the large inelastic deformations consistent with high ductility moment-resisting frames. Bayo et al [21] used a new component-based approach to model internal and external semi-rigid connections for the global analysis of steel and composite frames. The method is based on a finite dimensioned elastic–plastic four-node joint element that takes into consideration, in a congruent and complete way, its deformation characteristics (components in Eurocode), including those of the panel zone, and all the internal forces that concur at the joint.

As a consequence, this new element avoids the use of the β factor and the inherent iterative process that it requires. In addition, the eccentricities of the internal forces coming from the beams and columns that meet at the joint are also considered. Examples are solved that validate the new approach and demonstrate its efficiency. In addition, it is shown that when using the β factor the iterative process may not converge for elastic–plastic analysis. Moreover, the limitations imposed on β by EC3 and EC4 may lead to substantial errors in the internal forces and moments.

From the available literatures, it is noticed that although there are some research work toward finite element model of the composite construction, most of the work was towards the simulation of the structural behaviour of the composite beam, very few works have been done to the finite element modelling especially the 3-D models of the composite connections. As 2-D models have its limitation in accurately simulate the behaviour of the connection, a suitable 3-D finite element model is essential. In this paper, a 3-D model to simulate the behaviour of the composite joints has been built using ABAQUS. The model used 3-D continuum model incorporating contact with full non-linear material properties. It provided valuable understanding of the overall moment and rotation behaviour. The comparison of the model has been made with the test results, good agreement has been obtained.

2 Experimental studies

Eight full scale flush endplate composite joint tests with precast hollowcore slabs were conducted by Fu and Lam [1]. The variables are stud spacing, degree of the shear connections, area of the longitudinal reinforcement and slab thickness. All specimens were of cruciform arrangement as shown in Fig. 1 and to simulate the internal beam-column joints in a semi-rigid composite frame. The specimen was assembled from two 3300 mm long UB 457×191×89 kg/m grade S275 universal beams and one UC 254×254×167 kg/m grade S275 universal column to form the cruciform arrangement. The beams are connected to the column flanges using 10mm thick flush end plates with two rows of M20 Grade 8.8 bolts. The steel connection is a typical connection currently used in UK practice for simple joints. A single row of 19mm diameter headed shear studs are pre-welded to the top flange of the steel beams. Finally, two UB 305×102×28 kg/m universal beams were connected to the column web to make up of the full joint arrangement. Heavy columns were used in the tests, and the flange is very thick to ensure no plastic deformation is observed in the column. Full details of the test set up, instrumentation and material are described in the reference [1].

3. Three-dimensional finite element model

A three-dimensional finite element model consisting of three-dimensional continuum (solid) elements was created as shown in Fig.2 to simulate the composite joints with precast hollowcore slabs. A general-purpose finite element package ABAQUS is used for the simulation. The model replicates the composite joints from the experimental

program by Fu and Lam [1]. In order to reduce the computing time of the computer, only one side of the tests was simulated. The sizes of all the components except the precast slab are the same as the actual experimental work. The research conducted by El-Lobody et al. [12] showed that the effective breadth around the joint is confined to the in-situ infill concrete portion of the slabs as it is shown in Fig.4. And also, from Fig 2 & Fig.3 it can be seen that the longitudinal bar is placed only in the insitu concrete, the precast hollowcore unit is tied up by the transverse bars. Therefore, for the slab, only the in-situ infill concrete in the centre is modelled.

The boundary conditions and method of loading adopted in the finite element analysis follow closely those used in the tests. Material non-linearity was included in the finite element model by specifying a stress-strain curve in terms of the true values of stress and plastic strain. The incorporation of material nonlinearity in an ABAQUS model requires the use of the true stress (σ) versus the plastic strain (ε^{pl}) relationship, this must be determined from the engineering stress-strain relationship using

$$\sigma = \frac{F}{A} = \frac{F}{A_0}\frac{l}{l_0} = \sigma_{nom}(\frac{l}{l_0}) = \sigma_{nom}(1+\varepsilon_{nom})$$

The plastic data define the true yield stress of the material as a function of true plastic strain. The first piece of data defines the initial yield stress of the material and, therefore, should have a plastic strain value of zero. The strains provided in material test data used to define the plastic behaviour are total strains, but is not the plastic strains in the material which has to be decomposed into the elastic and plastic strain components. The plastic strain is obtained by subtracting the elastic strain which is defined as the value of true stress divided by the Young's modulus, from the value of total strain. This relationship is written

$$\varepsilon^{pl} = \varepsilon^{t} - \varepsilon^{el} = \varepsilon^{t} - \sigma / E$$

ε^{pl} Is true plastic strain

ε^t Is true total strain

ε^{el} Is true elastic strain

σ Is true stress, and

E Is Young's modulus

3.1 Material model of the steel components

All the structural steel components such as steel beams, steel columns, studs and bolts are modelled as an elastic-plastic material in both tension and compression. The stress-strains relationship in compression and tension are assumed to be the same. The classical metal plasticity model in ABAQUS defines the post-yield behaviour for most metals. ABAQUS approximates the smooth stress-strain behaviour of the material with a series of straight lines to simulate the actual material behaviour. Therefore, it is possible to obtain a close approximation of the actual material behaviour. As shown in Fig. 3, the material will behave as a linear elastic material up to yield stress of the material. After this stage, it will proceed into strain hardening stage until reach the ultimate stress. The elastic part of the stress-strain curve is defined with the *ELASTIC option, the value 2.1×10^5 N/mm^2 for the Young's modulus and 0.3 for the Poisson's ratio were used. The plastic part of the stress-strain curve is defined with the *PLASTIC option. The engineering stresses and strains including the yield and ultimate tensile strength obtained from the coupon tests were converted to true stresses and strains with appropriate input format for ABAQUS.

3.2 Endplate-column interaction

The observation from the tests [1] shows that initially, the beam and column are assembled together by means of the bolts. As load is applied to the structure, some parts of the endplate and the column flange separate whilst the remainder remained in contact. This behaviour is complicated to simulate as the members are not attached at all nodes along the boundary. To solve this problem, contact interactions were used with the *CONTACT PAIR option in ABAQUS. To simplify the model the weld between the endplate and the steel beam was not simulated and the nodes of the endplate are directly connected to the nodes of the steel beam. The general contact formulation used in ABAQUS involves a ‘master-slave’ type algorithm. With this approach the column flange surface was defined as the "master" surface and the endplate surface are defined as the "slave" surface. A kinematical constraint ensured that the slave surface nodes do not penetrate the master surface. The contacting surfaces need not have matching meshes. However, the best accuracy is obtained when the meshes are initially matching. For initially non-matching meshes, accuracy can be improved by judiciously specifying initial adjustments to ensure that all slave nodes that should initially be in contact are located on the master surface. Small-sliding contact is employed in the simulation which can undergo a relatively small sliding relative to each other and arbitrary rotation of the bodies is permitted. The small-sliding capability can be used to model the interaction between two deformable bodies or between a deformable body and a rigid body in two and three dimensions with less computational time but with little simulation difference in

comparison with finite sliding formulation. The normal contact pressure relationships between two faces are simulated with *HARD option which minimizes the penetration of slave nodes into the master surface and does not allow the transfer of the tensile stress across the interface. The friction between the endplate and the column was ignored as it is noticed that the friction is small during the test.

3.3 Simulation of bolted endplate connection

The mechanism of the bolted endplate connection is that the forces between the members are transferred through friction due to clamping between the members caused by the pretension force of the bolts. Many different approaches have been used by researchers in the past to simulate the bolt pretension force, bolt – endplate interface, and bolt – column flange interface. However, most of them are fairly complicated. Here, a new technique is proposed by the authors to model the interface. As shown in Fig.4, the bolts were made up of C3D8R elements. The shanks of the bolts were modelled as prismatic, having a diameter equal to the nominal bolt diameter of 20 mm. The details of the threads on the shank were neglected. A circular bolt head model that circumscribes the original shape and size of the M8.8 bolt was employed. Circular nuts were also modelled with the original size of the nuts. Both the head and the nuts are directly connected to the shank. The washers and thread are not modelled.

The nodes within each bolt head area on the bolted end plate are assumed to have the

same displacements in the finite element models. The nodes of the inner layer of elements on both the bolt head and the end plate were paired up and constrained using the *TIE option provided by ABAQUS [4]. With such an arrangement, both translational and rotational degrees of freedom of the tied nodes have the same displacements during the deformation process. The same arrangement is made to simulate the interaction between the nut and the column flange as well. The contact bearing interaction between the shank and the bolts hole are neglected. Using this method, the column flange and the endplate of the steel beam are confined by the two head of the bolt, (in the column side, the head is to simulate the nut in the tests), which preventing the separation of the endplate and the column flange before the actual separation. Actually, with the load applying, the shank of the bolt is in tension as the two ends of the bolt have been connected with the column flange and the endplate. However, some discrepancy will be made as the prestressed force in the shank affects the way components interact, so the accuracy of the model has been affected. However, by eliminating the simulation of the bolt pretension, this model presents a dramatic reduction in the computational time, and such inaccuracy is not significant to the overall behaviour of the model.

3.5 Longitudinal shear transmission mechanism.

In the simulation of the composite connections, another key issue is the longitudinal shear transmission mechanism. The longitudinal shear force is transferred to the concrete by dowel action of the connectors which results in the compression between

the connector and the concrete slabs. Through the bond interactions between the concrete and the longitudinal rebars, the shear force is transferred to the longitudinal rebars.

In the hogging moment regions, the concrete slab is mainly under tension. The full scale test results show that, in the initial loading stage, the concrete failed quickly after the application of the load and small cracks can be observed. However, the cracks of the concrete did not cause much deduction on the transmission of the longitudinal force between the studs and the rebars. This is because that the cracks always concentrate in some small area, the remaining of the concrete are still intact. In the plastic stage, the rotational stiffness of the connection deteriorated quickly after concrete cracks near the column flange have been formed throughout the depth of the slab. However, the concrete can still transmit longitudinal shear force through the shear stud to the longitudinal rebars to achieve higher moment capacity and rotation capacity. This is because that the cracked concrete may be subject to diagonal compressive strut action in between the top flange of the steel girder and the shear stud as shown in Fig.5. The concrete can anchor the studs into concrete up to failure.

Therefore, the key issue of the modelling is to simulate the mechanism of the longitudinal shear transmission, which related to the simulation of the reinforced concrete and the shear stud.

3.4 Modelling of reinforced concrete slabs

Two techniques exit so far for modelling reinforced concrete slabs: discrete and layered modelling. The first method is complicated and more expensive in term of analysis time. The second method is adopted in ABAQUS programs. Attempt has been made by the authors to model the slab with this method. It is capable of predicting the stiffness of the connection in the initial stage, but it terminates prematurely when concrete attained ultimate strength. The termination is possibly due to the impossibility of ABAQUS to simulate the large crack. The same problem was also reported by Baskar et al [11] and Ahmed [10]. To solve this problem, a discrete reinforced concrete slab model was established. As shown in Fig.6, both the slab and the reinforcing steel are modelled using C3D8R 3-D solid elements. The connectivity between the concrete nodes and the reinforcing steel nodes can be achieved by two methods: firstly, concrete and reinforcement share the same node; hence, perfect bond is assumed. Secondly, a spring element is used to connect concrete and the reinforcement nodes in order to simulate the bond-slip behaviour. As the bond slip is very small and can be ignored, the first method is adopted. To simplify the mesh, the longitudinal bar is simulated with rectangular section having the cross-sectional area of the actual steel bar used in the tests. The bond strength between the steel bar and concrete interaction is simulated as rigid connection using *TIE options by connecting the top face of the reinforcing bars and the concrete slabs.

3.5 modelling of shear stud connector

The shear connectors were simulated with the C3D8R 3-D solid elements. To simplify the mesh, it is simulated with rectangular section with cross-sectional area of the actual studs used in the tests and the head of the stud was not modelled. Fig. 7 is the moment vs. strain curve of 3 shear studs in Test CJ4 carried out by Fu and Lam [1]. Where, st11, st21 and st31 represent the strain gauge reading on the rear side of the studs and st12, st22 and st32 represent the strain gauge reading on the front side of the studs. It can be seen that in the front, the strain reading is negative, which means that the front side of the stud is in compressing due to the compressions between the studs and the slabs. At the back of the stud, the strain reading is positive which means that it is in tension and the stud is separating from the concrete slabs.

Therefore, in the simulation only the nodes of the studs at the front side are connected to the nodes of the concrete slab with rigid connection using *TIE options and the other nodes of the studs are detached to the surrounding concrete nodes. The same approach has been used by Kalfas et al [22] and El-Lobody et al [12] to avoid the interface elements needed to model the interaction between the stud and the concrete. As rigid connection is used, the anti-uplift function of the headed studs has also been simulated.

3.6 Concrete slab – steel beam Interface

From the test results it can be seen that the interface between the slab and steel beam flange can be considered as smooth with little friction. It is found by Baskar et.al [11]

and the authors that the connection of the node between the steel beam and the concrete slab will cause convergence problem in ABAQUS, therefore the steel beams and the slabs were modelled as separate elements during the simulation without any connection and contact elements. They were acting compositely only through the connection of the shear studs.

3.7 Material model for the concrete slabs

In the hogging moment regions, the concrete slab is mainly under tension. However, for the area around the front of the shear studs as shown in Fig.8 the concrete is in compression. The longitudinal shear force is transferred between the shear studs and the concrete slabs. As the convergence problem of ABAQUS to simulate the concrete material after cracking, a simplified elastic-plastic material model was adopted here to simulate the concrete slabs as shown in Fig.9. It is assumed that the concrete behaves as a linear-elastic material up to the yield. The option *PLASTIC is used to specify the plastic part of the material model that use the Von Mises yield surface. For the elastic part of the stress-strain curve, the value of the Young's modulus and the Poisson's ratio of the concrete are determined in accordance to BS8110 [23]. For the plastic part, it is required to identify the yield stress. Two different values are adopted in different area of the slab. The main area of the concrete slab as shown in Fig. 8 is defined with the ultimate tensile stress f_t which is obtained from the concrete indirect tensile test. As shown in Fig.8, the area with 4×d length and 1.5 d width and the same height of the stud in the compressive side of the stud is defined with the yield stress 0.8 f_{cu} which is obtained from concrete cube tests. The ultimate compressive strain ε_{cu}

is given as 0.002ε. Although the proposed material model for the concrete can not predict the explicitly crack initiation and the evolution, the modelling result shows that it is sufficiently accurate for simulating the behaviour of the composite connection.

In this model, only in-situ concrete infill was modelled. The precast slab and the transverse bar are not modelled. The reason for this simplification is that the test results show that during the test, the strain reading of the transverse bar was quite small and remained elastic. So, the transverse bar has little effect on the connection capacity. The effective width of the composite connection is taken as the width of the in-situ concrete infill and the precast hollowcore slabs are ignored.

3.8 Boundary condition and Load conditions

For the boundary conditions, all the concrete nodes and the longitudinal rebar nodes at the connection side are restricted as fixed as only one side of the composite beam is simulated. The bottom of the column was fixed in order to simulate the column base plates. A static concentrate load is applied on the end of the steel beam at the centre of the steel flange as shown in Fig.2. The increment of the load is applied using the modified RIKS method available in the ABAQUS.

4. Validation of the finite element model

To validate the accuracy of the model, the FE analysis results are compared with the test results. Table 1 is the test arrangement and mode of failure of the eight full scale tests. Comparisons have been made for moment-rotation curve, moment-beam bottom

flange strain curve, moment-slip curve and moment-rebar strain curves.

4.1 Moment- Rotation curve comparison

The comparisons are shown in Table 2, Table 3 and Fig.10-17. It can be seen that except CJ3, the numerical results have good agreement with the tests data. This is because that the mode of failure of CJ3 is due to the premature failure of concrete slab splitting near one of the studs. As the FE model uses the elastic-plastic material properties to simulate the concrete slab, it could not properly simulate the compressive failure of the concrete due to the interaction between the slab and the stud, as the concrete will continue deforming over the ultimate compressive stress. The mode of failure of the FE model CJ3 is due to the shear failure of the stud. The model can accurately simulate the initial stiffness of the moment-rotation curve. For the plastic part of the curve, the modelling result is slightly larger. The reason is that in the simulation, in the elastic stage, the actual Young's modulus and the Poisson's ratio of the tests are chosen in the material model to simulate the concrete material, so there is little difference. In the plastic stage, the slab actually does not have much contribution to the moment capacity after cracking in the actual tests. However, as the slab is modelled with the elastic-plastic material, so after concrete attaining the ultimate tensile strength, the simulated slab can still contribute to the moment capacity as it will deform continuously. Therefore, higher moment capacity is resulted, but as only the in-situ concrete is modelled, the discrepancy is quite small. The modelling results also show a larger rotation capacity. The discrepancy is because in

the simulation perfect bond interface between the steel bar and the concrete slab has been presumed and the bond slip has been ignored. The tension stiffen effect of the concrete is also ignored. Therefore, after the slab is cracked, the connection between the steel bar and the slab is maintained in the model, though due to the tension stiffening effect, the embedded reinforcement has a lower overall ductility than bare reinforcement.

4.2 Moment- Rebar strain curves

The strain along the longitudinal bar in the FE model is chosen from the same position as the strain gauge position in the tests. Fig 18 shows comparison results between the Test CJ1 and the FE-solution. It can be seen that the model can accurately simulate the strain of the longitudinal rebars.

4.3 Moment-beam bottom flange strain curve

In the full scale tests, the strain was measured at the point 100 mm away from the column face on the upper surface of the steel beam. Results from the FE modelling were extracted from the same position and the comparison was made. As shown in Fig.19. It can be seen that, the model can accurately simulate the moment-strain curve of the test.

4.4 Moment- Slip curve comparison

In the full scale tests, LVDT has been placed on the steel beam to measure the slip between the steel beam and the precast slab. The same slip has been measured at the

first stud position from model CJ5. Fig.20 shows the comparison between the modelling results and the test results. It can be seen that the model can predict the maximum slip between the slab and the steel beam accurately.

4.5 Mode of failure

As shown in Figs 21, the proposed model can also accurately simulate plastic deformation of the endplate. And also, two mode of failure has bean noticed:

a) Yielding of shear studs. Fig.22 is the FE model CJ3 at the failure state. It can be seen that the large deformation of the stud is observed. And also, the stress contour shows the yielding of the stud.

b) Yielding of the longitudinal rebars. Fig 23 is the FE model CJ1 at the failure state. It can be seen from the stress contour of the two longitudinal rebars that, the two rebar are yielding.

Table 4 is the failure mode comparison between the full scale tests and the modelling results. It can be seen that, except CJ3, the model can predict the mode of failure of all the tests.

4.6 recommendations

The paper is entirely devoted to the beam to column connection (including the relevant part of the slab). But, the structural designers are interested with the whole structure. For the full analysis of the global structure, the simplified model is

suggested , as the refined model suggested in this paper is computational expensive for a global structure. The connection can be modelled using component method with the use of the spring element. The studs can also be simulated using the spring element. However, the determination of the spring stiffness need to be calibrated against the refined model in this paper and the full scale test. Although full scale tests is the best option but due to the cost, the refined model is a better alternative.

5. Conclusion

In this paper, a 3-D finite element model was firstly built using 3-D continuum element with the ABAQUS package to simulate the behaviour of the semi-rigid composite connection with precast hollowcore slabs. The methodology for the modelling techniques is described in details. The relationship between all the components are explicitly modelled using contact elements. The model also incorporates nonlinear material characteristics and non-linear geometric behaviour. A simplified method to simulate the bolted end plate connection is introduced. The simulation method of the longitudinal shear transmission is proposed which can accurately simulate the plastic state of the longitudinal rebars after cracking. Different materials are chosen by the authors to simulate the concrete slab. The elastic-plastic material properties are adopted to simulate the slab as which can accurately simulate the moment-rotation response of the connections. All the numerical results are presented and compared to experimental data and good agreement is obtained. The comparison between the modelling results and the eight full scale tests results shows

that except test CJ3, the model can predict the full moment-rotation response of the composite connections in a small discrepancy. It can also properly simulate the actual behaviour of the endplate connection. The model is able to predict the behaviour and the mode of failure of all the tests.

6. Acknowledgement

The authors would like to acknowledge the financial support from International Precast Hollowcore Association (IPHA) and Overseas Research Scholarship (ORS), the support provided by Severfield – Revee Structures Ltd. for supplying the steel specimens and Bison Concrete Products Ltd. for supplying the precast hollowcore slabs.

7. References

[1] Fu F. and Lam D., Experimental Study on Semi-Rigid Composite Joints with Steel Beams and Precast Hollowcore Slabs, Journal of Constructional Steel Research Volume 62, Issue 8 , August 2006, Pages 771-782

[2] Krishnamurthy N., Modelling and prediction of steel bolted connection behaviour. Computers and Structures, Vol. 11, 1979, pp. 75–82.

[3] Krisbnamurthy, N. and Graddy, D., Correlation between 2- and 3-dimensional finite element analysis of steel bolted end-plate connections, Computers and Structures, Vol. 6, 1976, pp. 381-389.

[4] ABAQUS theory manual, version 6.4. Hibbitt, K-arlsson and Sorensen. Inc., Pawtucket, R.I., 2003

[5] Bursi O. S. and Jaspart J. P., Basic issues in the finite element simulation of extended end plate connections, Computers & Structures, Vol. 69, Issue 3,

November, 1998, pp. 361-382

[6] Choi C. K. and Chung G. T., Refined Three-Dimensional Finite Element Model for End-Plate Connection, J. Struct. Eng., Vol. 122, 1996, pp. 1307 - 1316

[7] Ayoub A. and Filippou F. C., Mixed formulation of nonlinear steel–concrete composite beam element, J. Struct. Eng., Vol. 126 (3), 2000, pp. 371–381.

[8] Sebastian W. M. and McConnel R. E., Nonlinear FE analysis of steel-concrete composite structures, J. Struct. Eng., Vol. 126, (6), 2000, pp. 662–674.

[9] Fabrrocino G., Manfredi G. and Cosenza E., Analysis of continuous composite beams including partial interaction and bond, J. Struct. Eng., Vol. 126, 2000, pp. 1288–1294.

[10] Ahmed B., Numerical Modelling of Semi-rigid Composite Joints, Ph.D. thesis, 1996, University of Nottingham, U.K.

[11] Baskar K., Shanmugam N.E., Thevendran V Finite-element analysis of steel-concrete composite plate girder, Vol. 128, No. 9, 2002, pp.1158 – 1168

[12] El-Lobody, E. and Lam, D., 'Modelling of headed stud in steel – precast composite beams', Steel & Composite Structures, Vol. 2, No. 5, 2002, pp. 355-378.

[13] Ju, S.H., Fan C. Y.,Wu G.H. Three-dimensional finite elements of steel bolted connections, Engineering Structures Vol. 26 2004 pp 403 – 413

[14] Vigh L. G., Dunai L., Finite element modelling and analysis of bolted joints of 3D tubular structures Computers and Structures Vol. 82 (2004) pp 2173 – 2187

[15] Kumar S.R.S., Rao D.V. P., RHS beam-to-column connection with web opening—experimental study and finite element modelling, Journal of Constructional Steel Research, Volume 62, Issue 8 , August 2006, pp 739-746

[16] Anderson, D, Composite steel-concrete joints in braced frames for buildings, Semi-rigid behaviour of Civil Engineering structural connections, COST C1, Brussels, Luxembourg, 1999

[17] Jaspart, J.P Recent advances in the field of structural steel joints and their representation in the building frame analysis and design process, Semi-rigid behaviour of Civil Engineering structural connections, COST C1, Brussels, Luxembourg, 1999

[18] Eurocode 3, Design of steel structures — Part 1.8 Design for joints, Joints in building frames, BS EN 1993-1-8:2005.

[19] Eurocode 4, Design of composite steel and concrete structures—Part 1.1 General rules and rules for buildings, ENV 1994-1-1:1992.

[20] Braconi A., Salvatore W., Tremblay R. and Bursi O. S., Behaviour and modelling of partial-strength beam-to-column composite joints for seismic applications EARTHQUAKE ENGINEERING AND STRUCTURAL DYNAMICS. 2007; Vol.36 pp142–161

[21] Bayo E., Cabrero J.M. and Gil B. An effective component-based method to model semi-rigid connections for the global analysis of steel and composite structures, Engineering Structures, Volume 28, Issue 1 , January 2006, pp 97-108

[22] Kalfas C., Pavlidis P. and Galoussis E., Inelastic behaviour of the shear connection by a method based on FEM, Journal of Constructional steel research, Vol. 44, Nos 1-2,1997, pp 107 - 114

[23] BS 8110 Part 1 Structural use of concrete —Part 1: Code of practice for design and construction, British Standards Institution, London, 1997.

Figures:

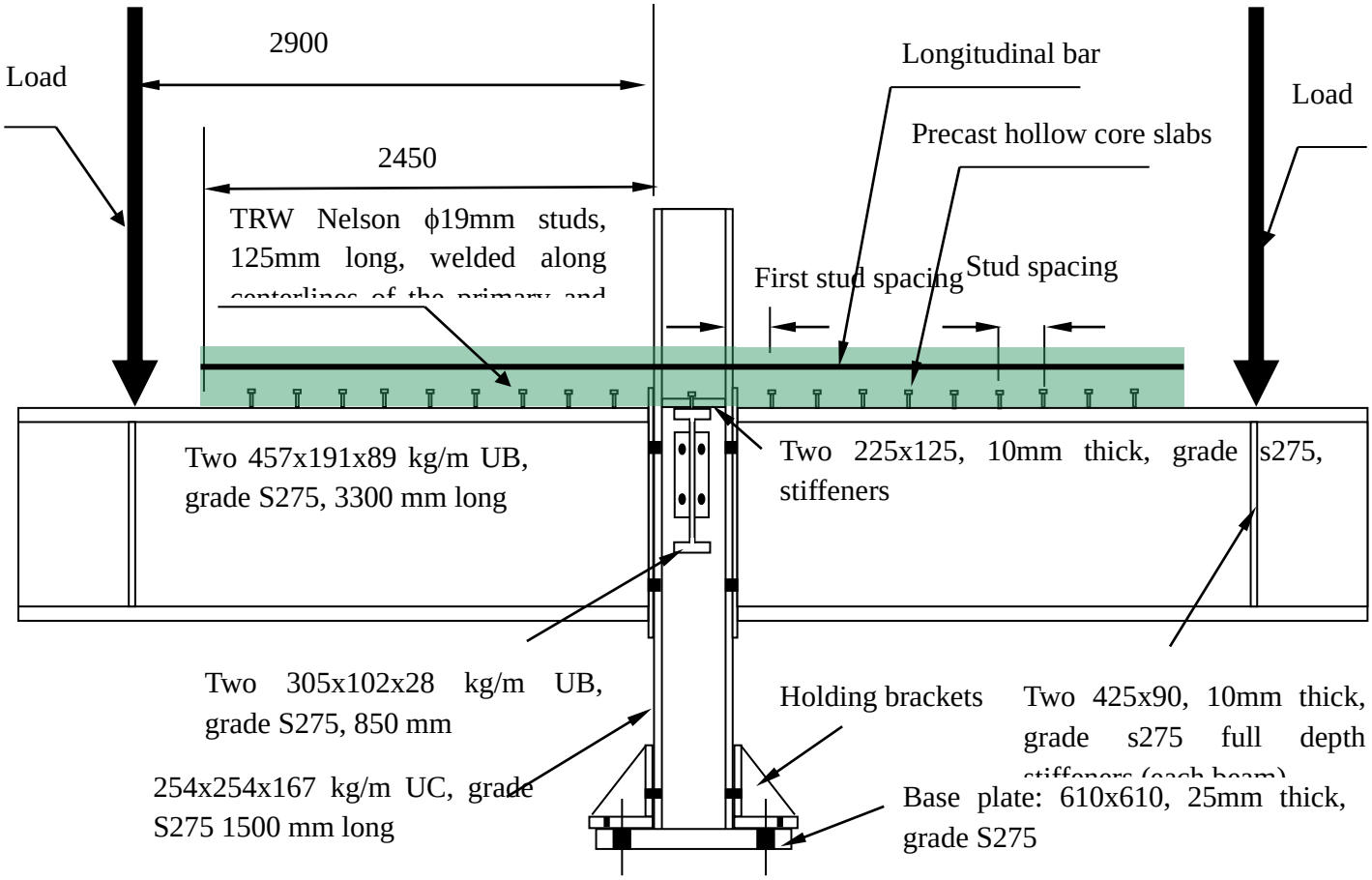

Fig 1 Composite connection test by Fu and Lam [1]

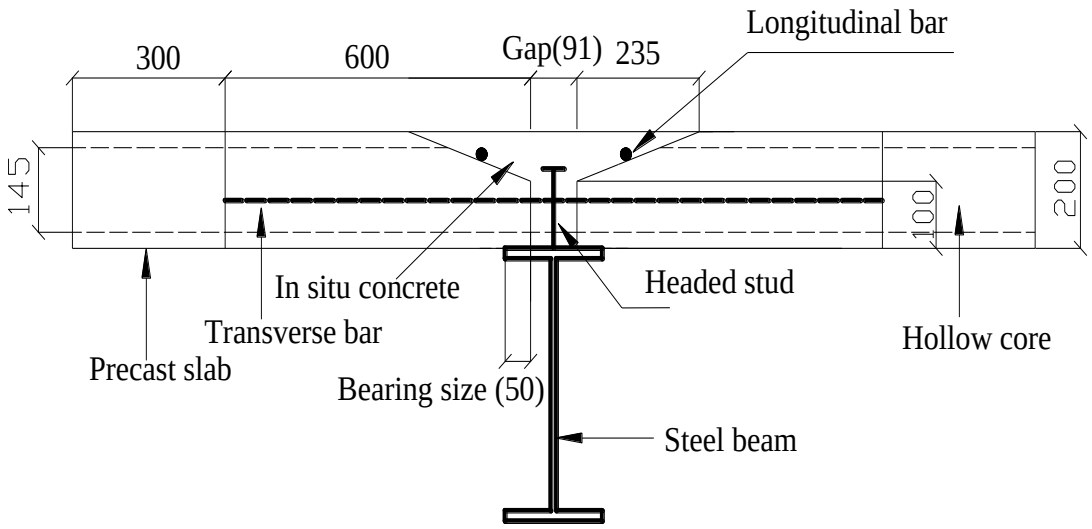

Fig 1 Cross section of composite beam

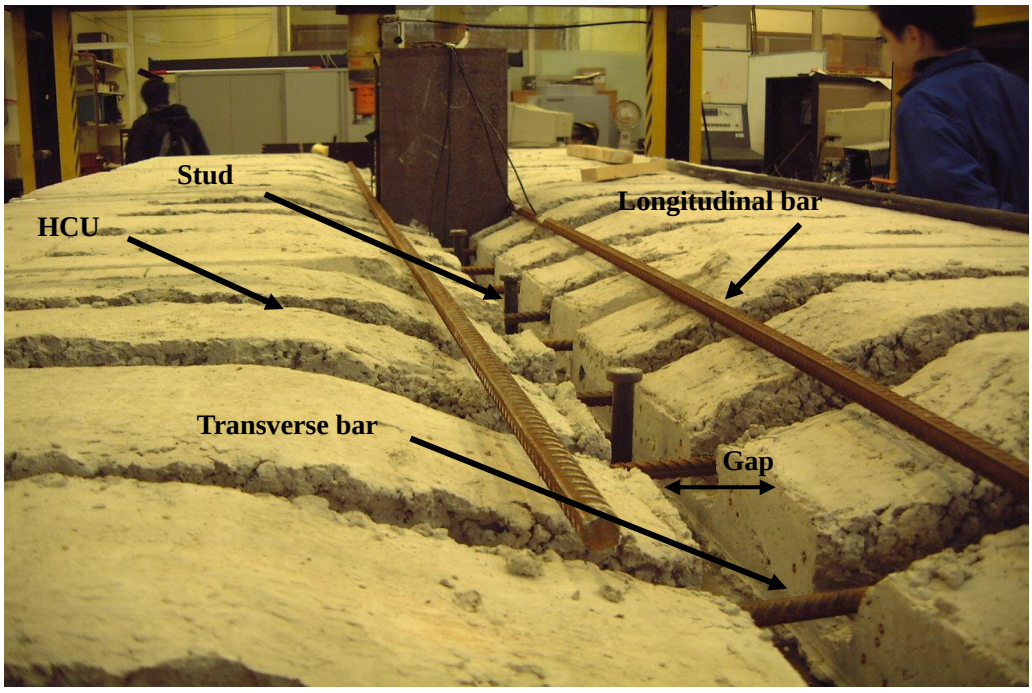

Fig 3 Slab, Longitudinal bar, Stud, Transverse Bar before casting

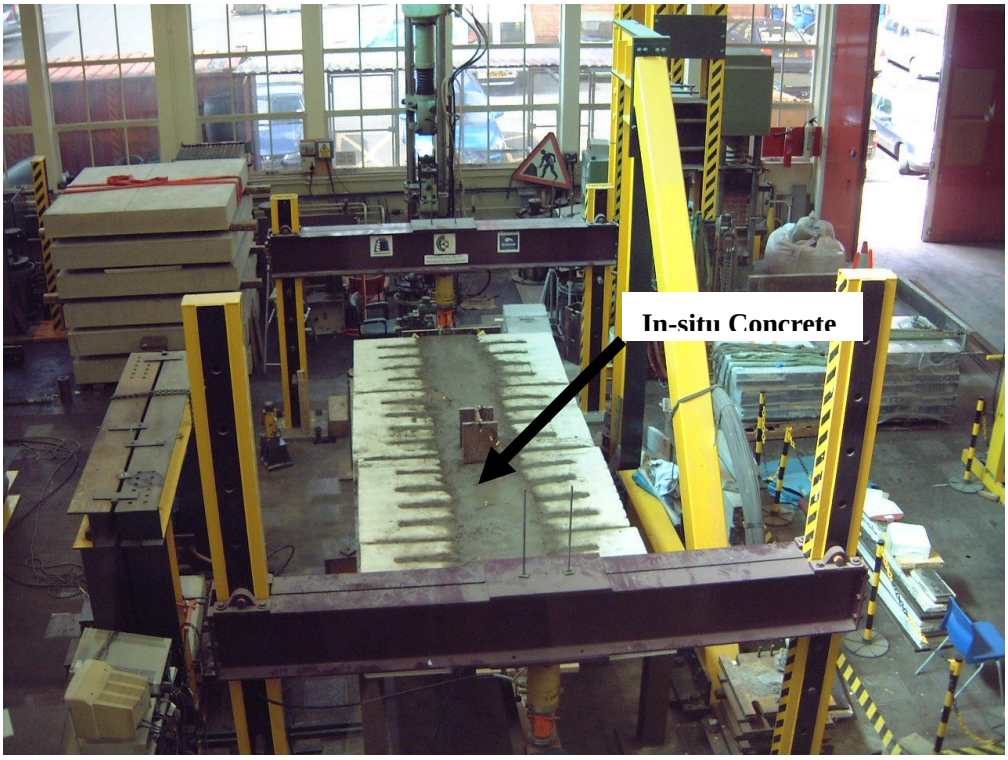

Fig 3 Testing rig after casting

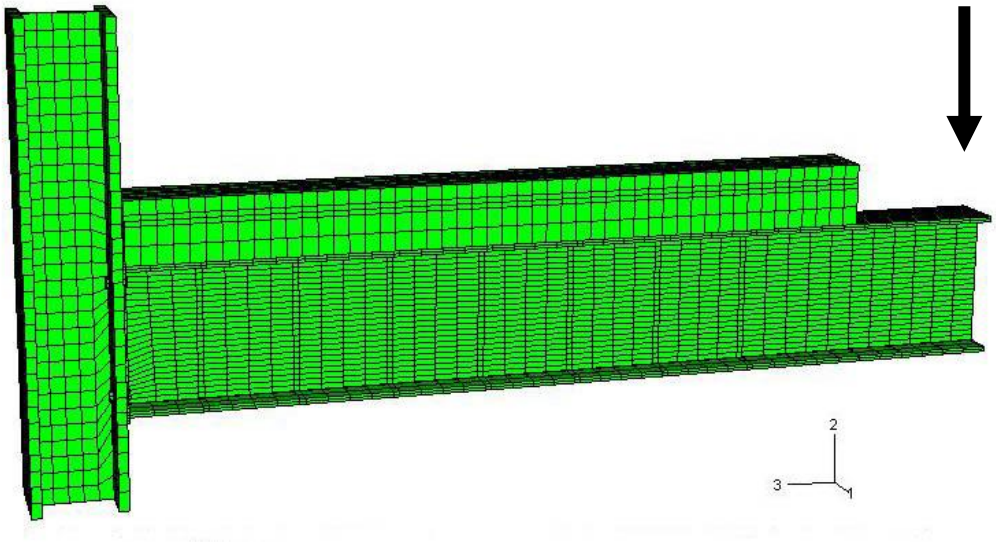

Fig 4 3-D finite element model of composite connection

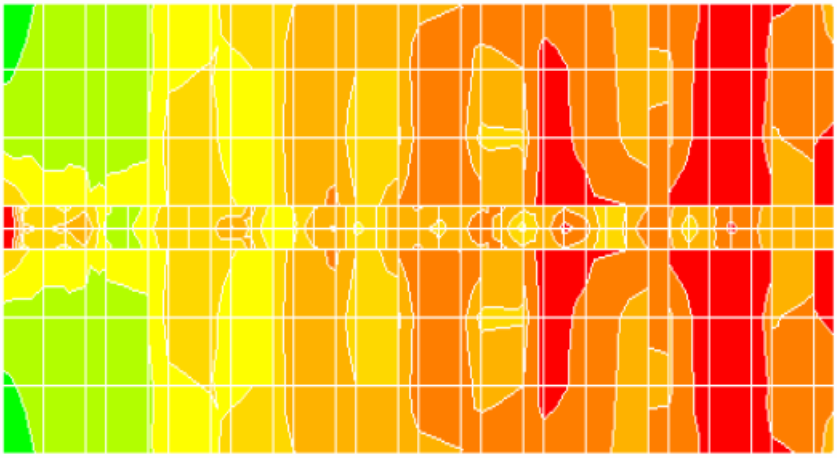

Fig.5 Effective width of composite beam using precast slab

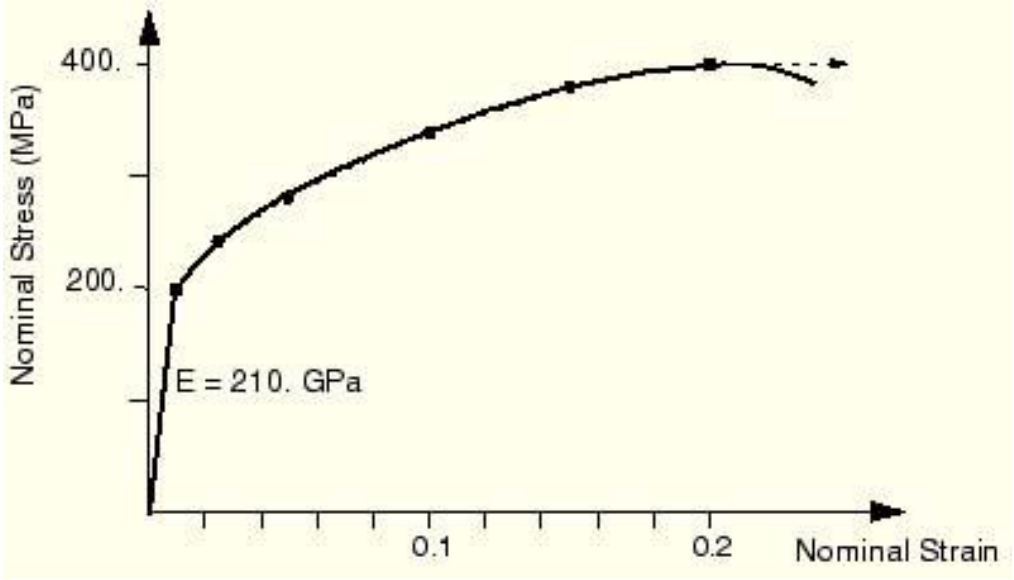

Fig.3 Elastic-plastic material behaviour by ABAQUS 6.4

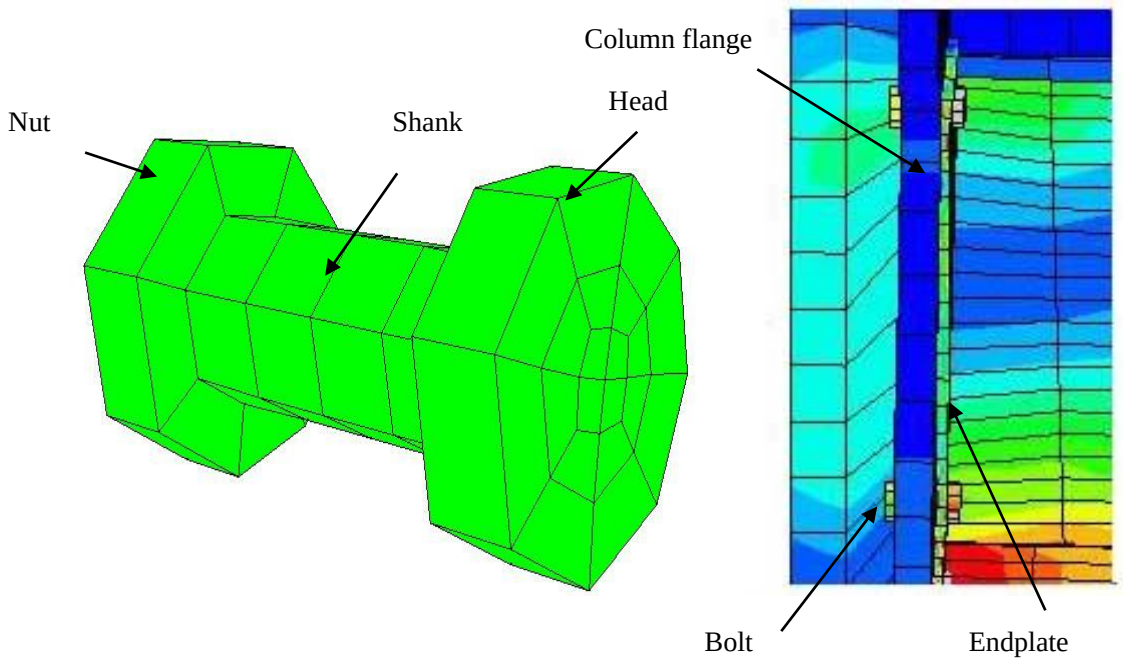

Fig. 4 Bolted endplate connection model

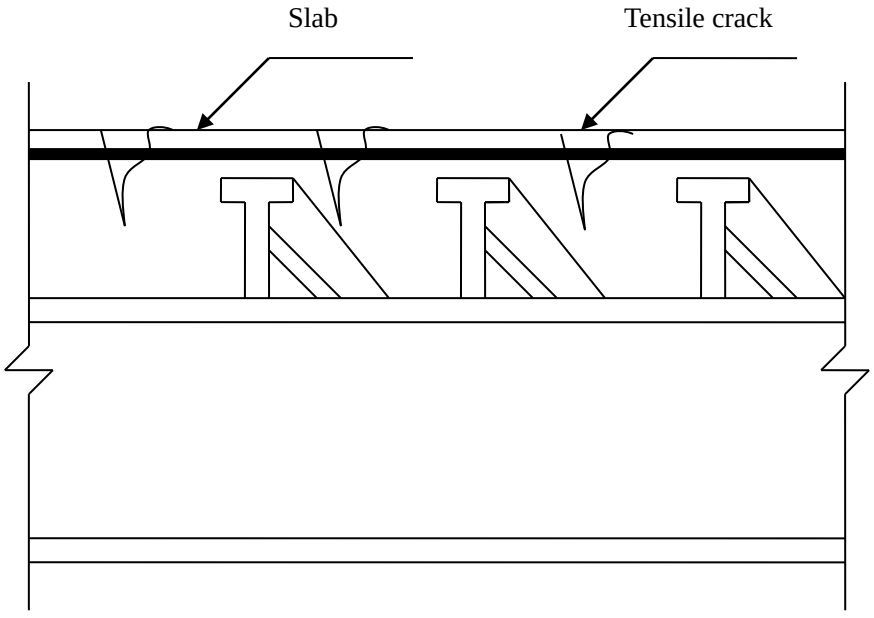

Fig 5 diagonal compressive strut action of cracked concrete

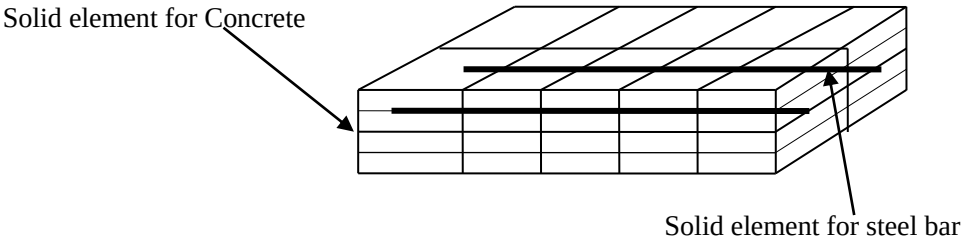

Fig. 6 Discrete modelling of reinforced concrete slabs

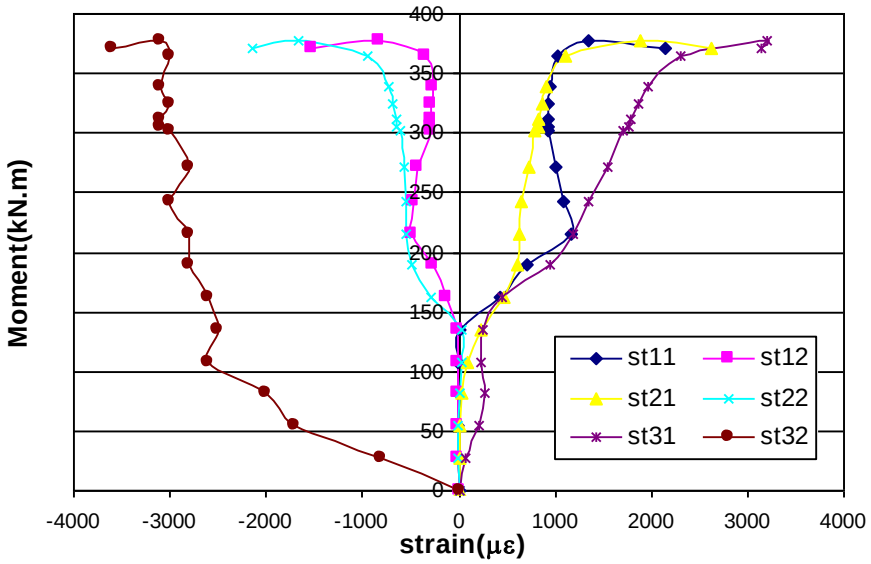

Fig. 7 strain vs. moment curve of the shear stud for tests CJ4

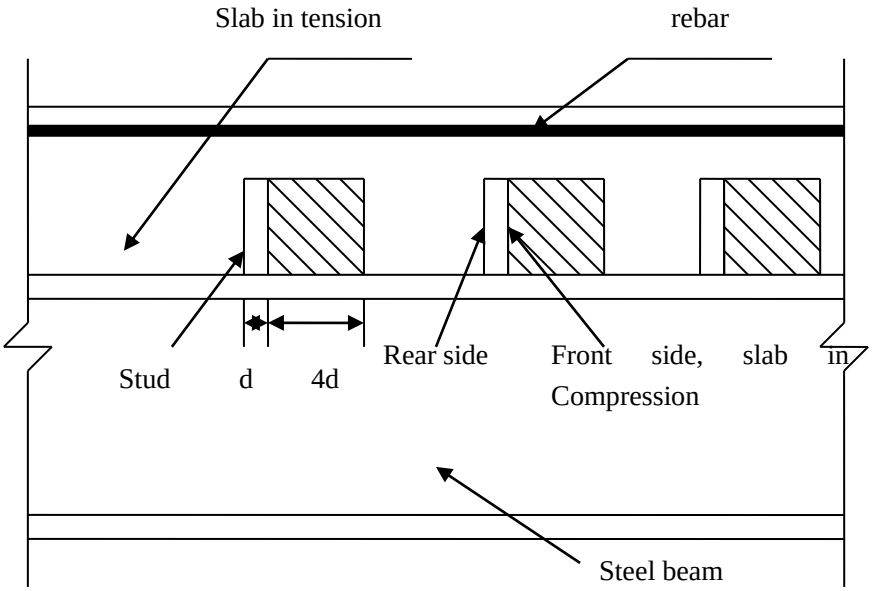

Fig. 8 the composite construction model

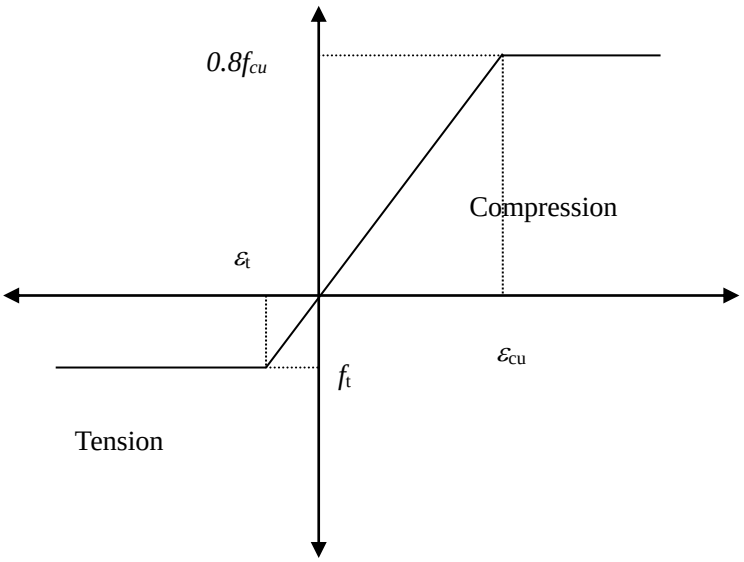

Fig. 9 the material model of the concrete

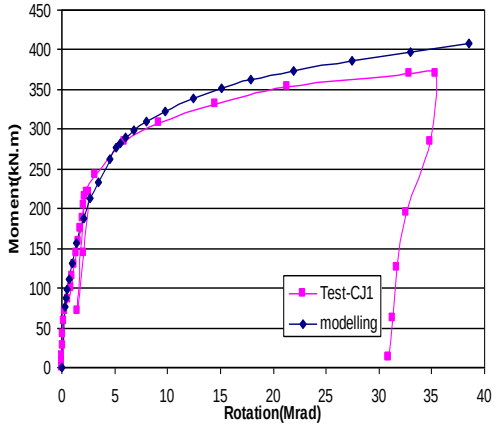

Fig. 10 Moment vs. rotation curves for test CJ1 and FE-solution

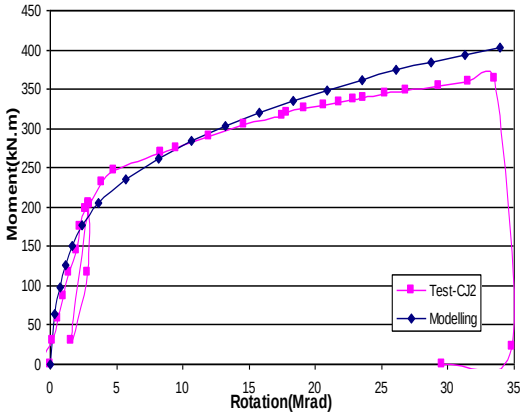

Fig. 11 Moment vs. rotation curves test CJ2 and FE-solution

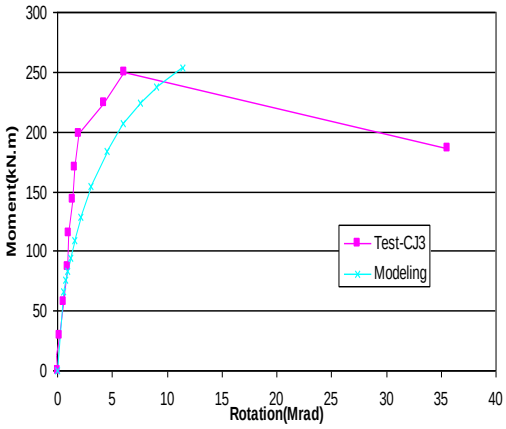

Fig. 12 Moment vs. rotation curves for test CJ3 and FE-solution

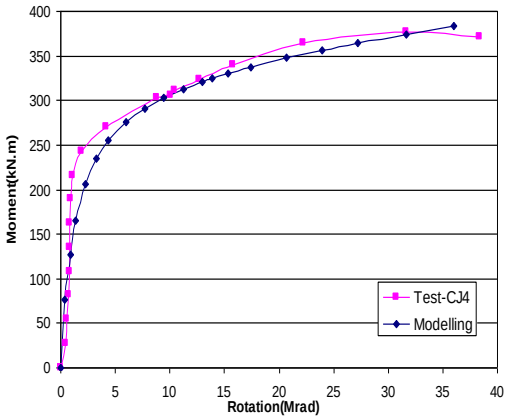

Fig. 13 Moment vs. rotation curves for test CJ4 and FE-solution

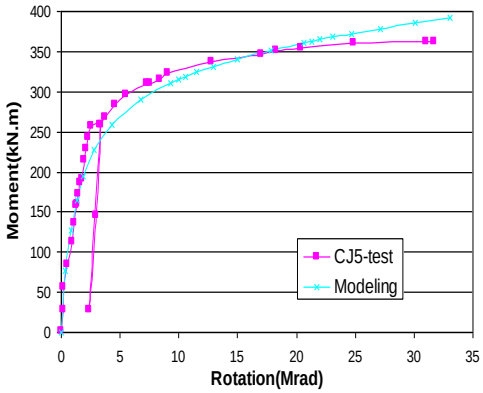

Fig. 14 Moment vs. rotation curves for test CJ5and FE-solution

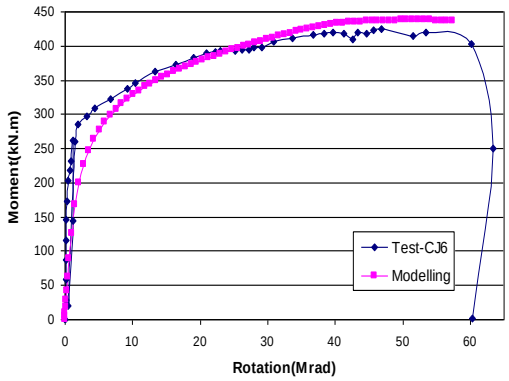

Fig. 15 Moment vs. rotation curves for test CJ6 and FE-solution

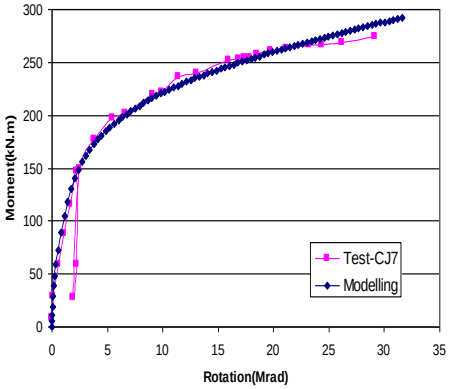

Fig. 16 Moment vs. rotation curves for test CJ7 and FE-solution

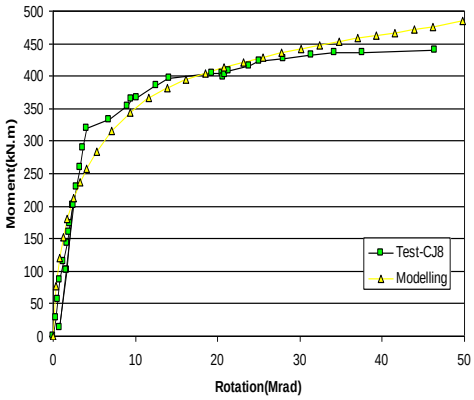

Fig. 17 Moment vs. rotation curves for test CJ8 and FE-solution

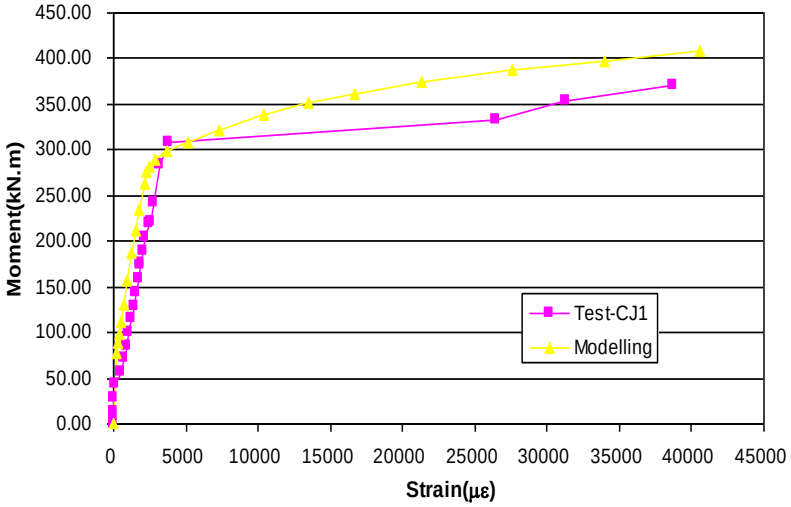

Fig 18 is Moment vs. strain of the longitudinal bar curves for test CJ1 and FE-solution

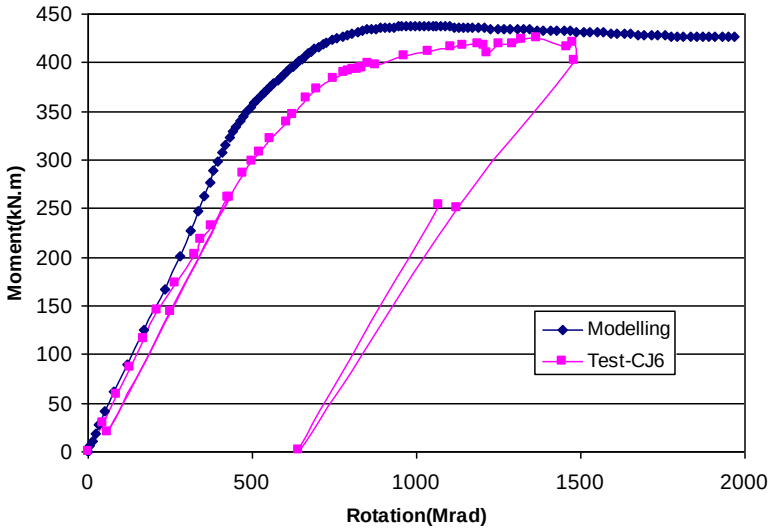

Fig 19 Comparison of moment-beam bottom strain curves

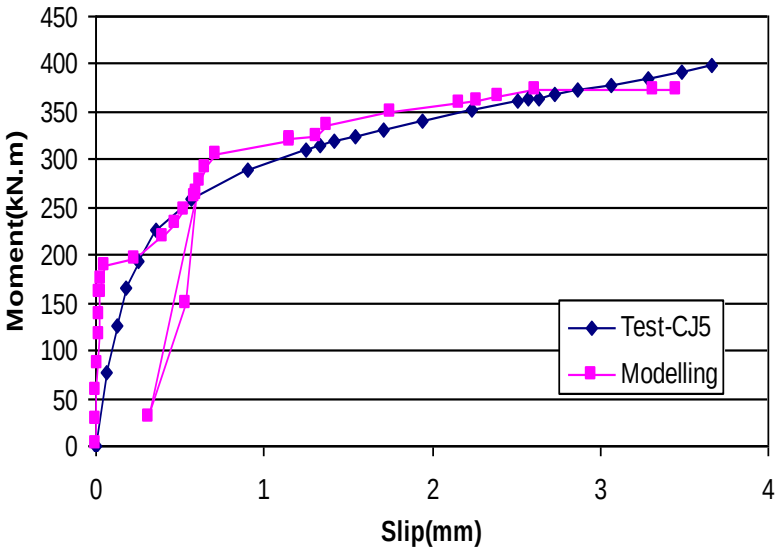

Fig.20 Comparison of moment- first stud slip curve

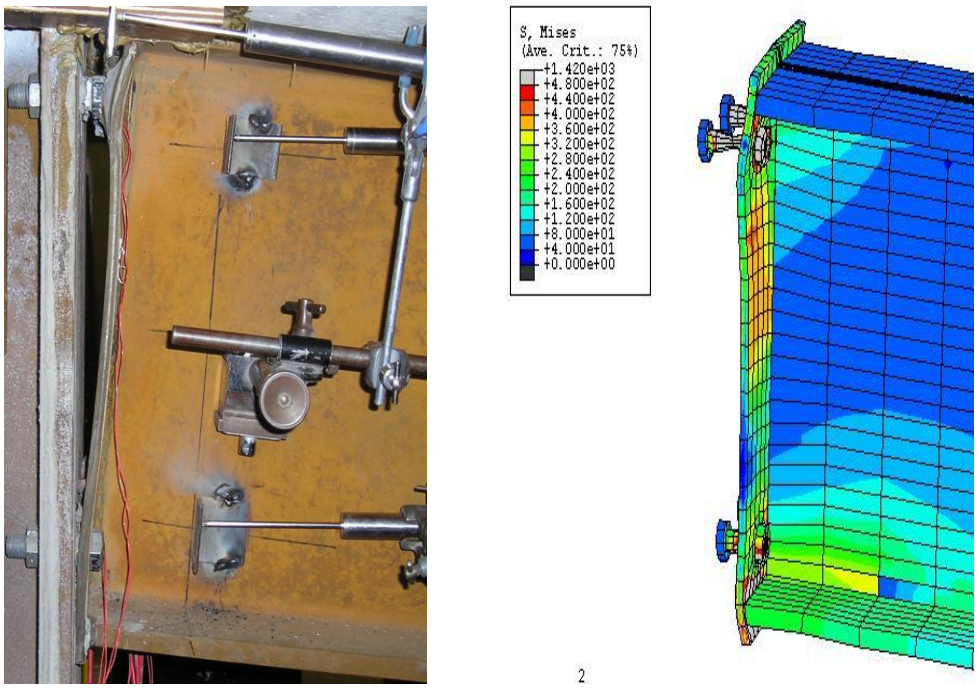

tests 3-D simulation

Fig. 21 Endplate deformation at the plastic failure state

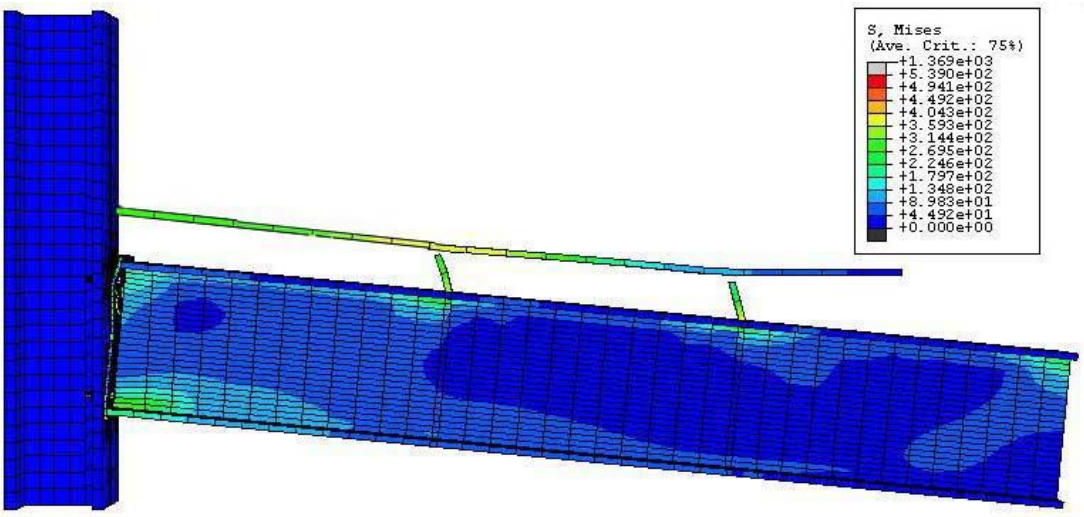

Fig. 22 Stud failure of CJ3 modelling (without showing slab)

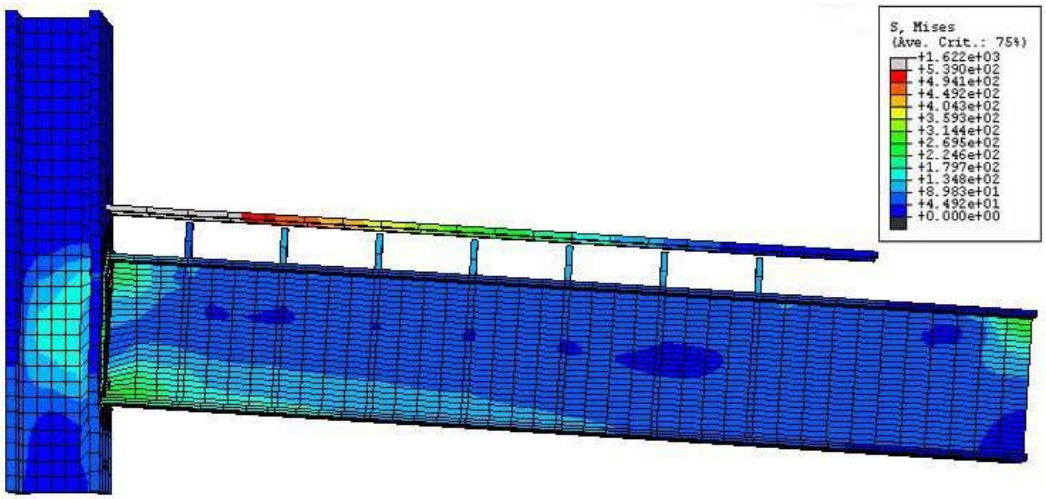

Fig. 23 Longitudinal bar failure of CJ1 modelling (without showing slab)

Tables:

Table 1 Tests arrangement

Ref.	Slab thickness (mm)	Longitudinal bars	Headed shear studs (mm)	Studs spacing (mm)	Position of first stud (mm)	No. of shear connector per beam	Mode of failure
CJ1	200	2 T20	19ϕ × 125	300	235	7	RF
CJ2	200	2 T20	19ϕ × 125	600	235	4	RF
CJ3	200	2 T20	19ϕ × 125	900,1200 [a]	990,540 [a]	2	Slab
CJ4	200	2 T20	19ϕ × 125	400	510,710[a]	3	CF
CJ5	200	2 T20	19ϕ × 125	500	645	3	CF
CJ6	200	4T16	19ϕ × 125	310	465	6	RF
CJ7	200	2T16	19ϕ × 125	1200	900	2	RF
CJ8	250	4T16	19ϕ × 125	450	705	4	RF

[a] stud on the east side

RF – reinforcement fracture; CF – connector fracture; SF – slab shear failure

Table 2 comparison of moment capacity

Reference	CJ1	CJ2	CJ3	CJ4	CJ5	CJ6	CJ7	CJ8
Test result (kNm)	370	363	250	368	363	425	274	439
3-D modelling result (kNm)	407	402.9	253.7	383	398	437.6	292	475

Table 3 comparison of rotation capacity

Reference	CJ1	CJ2	CJ3	CJ4	CJ5	CJ6	CJ7	CJ8
Test result (mrad)	34.3	33.5	6.1	31.6	31	46.8	30	46.4
3-D modelling result (mrad)	38.5	33.9	11.5	36	36.1	51.4	31.5	49.7

Table 4 comparison of failure mode

Reference	CJ1	CJ2	CJ3	CJ4	CJ5	CJ6	CJ7	CJ8
Test result (kNm)	RF	RF	Slab	CF	CF	RF	RF	RF
3-D modelling result (kNm)	RF	RF	CF	CF	CF	RF	RF	RF

RF – reinforcement fracture; CF – connector fracture; SF – slab shear failure